A Micromechanic Study of Cell Polarity and Plasma Membrane Cell Body Coupling in *Dictyostelium*

Rudolf Merkel,* Rudolf Simson,* Doris A. Simson,* Melanie Hohenadl,* Alexei Boulbitch,* Eva Wallraff,† and Erich Sackmann*

*Fakultät für Physik, Lehrstuhl für Biophysik, Technische Universität München, D-85747 Garching, and †Max-Planck-Institut für Biochemie, D-82152 Martinsried, Germany

ABSTRACT We used micropipettes to aspirate leading and trailing edges of wild-type and mutant cells of *Dictyostelium discoideum*. Mutants were lacking either myosin II or talin, or both proteins simultaneously. Talin is a plasma membrane-associated protein important for the coupling between membrane and actin cortex, whereas myosin II is a cytoplasmic motor protein essential for the locomotion of *Dictyostelium* cells. Aspiration into the pipette occurred above a threshold pressure only. For all cells containing talin this threshold was significantly lower at the leading edge of an advancing cell as compared to its rear end, whereas we found no such difference in cells lacking talin. Wild-type and talin-deficient cells were able to retract from the pipette against an applied suction pressure. In these cells, retraction was preceded by an accumulation of myosin II in the tip of the aspirated cell lobe. Mutants lacking myosin II could not retract, even if the suction pressures were removed after aspiration. We interpreted the initial instability and the subsequent plastic deformation of the cell surface during aspiration in terms of a fracture between the cell plasma membrane and the cell body, which may involve destruction of part of the cortex. Models are presented that characterize the coupling strength between membrane and cell body by a surface energy σ. We find $\sigma \approx 0.6(1.6)$ mJ/m^2 at the leading (trailing) edge of wild-type cells.

INTRODUCTION

Various cellular processes are controlled by the viscoelastic properties of the cell envelope, a composite stratified shell comprising the lipid/protein bilayer and the associated actin/myosin cortex. Prominent examples are cell adhesion (Sackmann, 1995; Evans, 1995) and ameboid locomotion on substrates (Oster and Perelson, 1987; Bray and White, 1988; Condeelis, 1993a,b). Thus recent comparative studies on the adhesion of vesicles and cells of *Dictyostelium discoideum* have shown that the adhesion strength (or the free energy of unbinding) of these soft shells is determined in part by the bending stiffness of the cell envelope and the lateral tension of the membrane (Simson et al., 1997). This correlation between adhesion strength and membrane elasticity is a consequence of the control of the shape of adhering soft shells by the mechanical equilibrium at the cell-substrate contact zone (Seifert and Lipowsky, 1990; Bruinsma, 1996). Therefore, reduction of the bending stiffness of the cell envelope by removal of actin-binding proteins (e.g., gelation factors) can drastically impede the crawling motion of cells on substrates exerting weak adhesion forces, such as mica (Schindl et al., 1995). Newly formed pseudopods cannot adhere strongly enough to allow retraction of the trailing end, and they are retracted again if new pseudopods are formed at another side of the cell. In addition to this mechanism, knockout of gelation factors reduces cortical stability and thus impedes locomotion because newly formed pseudopods cannot be sufficiently stabilized (Cunningham et al., 1992; Cunningham, 1995).

An interesting correlation between the deformability of the composite membrane and adhesion has clearly been demonstrated by comparative measurements of the free energy of adhesion, the membrane tension, and the bending elastic modulus of wild-type cells and mutants of *Dictyostelium* by microinterferometry in combination with a hydrodynamic shear field deformation technique (Simson et al., 1998). In this study, talin-null mutants exhibited a reduction of the bending stiffness by a factor of 5–6 compared to wild-type cells. Because talin is well known to mediate the coupling between actin cortex and the bilayer membrane in many cell types (Horwitz et al., 1986; Isenberg and Niggli, 1998), these experiments demonstrate that the elasticity of the cell envelope is controlled to a great extent by the coupling strength between the actin cortex and the membrane.

To gain further insight into the control of cellular shape changes (e.g., during locomotion) by the viscoelastic properties of the cell envelope that are regulated in turn via the coupling of the actin/myosin cortex to bilayer and intracellular cytoskeleton, respectively, we performed the following micropipette aspiration experiments. Adherent cells were aspirated locally into the pipette, and the resulting equilibrium length of an aspirated cell portion was measured as a function of the suction pressure. To establish a possible intrinsic polarity of the moving cells, these aspiration lengths were measured at the leading edges where new pseudopods started to form and at the opposite ends (referred to as the trailing edge). Four types of *Dictyostelium* cells were studied: wild-type cells, myosin-null mutants,

Received for publication 3 June 1999 and in final form 9 May 2000.

Address reprint requests to Dr. Erich Sackmann, Physik Department E22, Technische Universität München, James-Franck-Str. 1, D-85747 Garching, Germany. Tel.: 49-89-2891-2471; Fax: 49-89-2891-2469; E-mail: sackmann@ph.tum.de.

0006-3495/00/08/707/13 $2.00

talin-null mutants, and double mutants lacking both of these actin-binding proteins. In a second series of experiments we studied the distribution of myosin II and actin in the enforced protrusions of wild-type cells transfected with fusion proteins consisting of green fluorescent protein (GFP) and actin or myosin II, respectively.

The pertinent results of this study are as follows:

1. Protrusion of the cell into the pipette requires a threshold suction pressure, P_{th}. The average threshold pressures of all cell types containing talin are remarkably smaller at the leading edge than at the trailing edge, pointing to a weakening of the cell envelope at the leading edge. The threshold pressure at both the leading and the trailing edges is larger by a factor of ~5 for myosin-deficient cells and for double mutants as compared to wild-type cells. In contrast, the removal of talin yielded different effects for leading and trailing ends of cells. No remarkable effect on the value of P_{th} at the cell front could be observed; a markedly reduced P_{th} was observed at the cell end.

2. Application of suction pressures exceeding a threshold pressure P_{th} leads to the protrusion of the cells into the pipette until an equilibrium length of the aspirated cell lobe, referred to as the projection length L_p, is reached. The aspiration length correlates roughly with the suction pressure. However, it varies strongly between different sites on the cell surface and for different cell types.

3. The ratio of projection lengths L_p and suction pressure P for myosin-null mutants and the double mutants is smaller by about an order of magnitude than the values obtained for wild-type cells and talin-null mutants.

4. Suction-enforced protrusion of wild-type cells is a transient phenomenon. About 20 s after reaching the equilibrium projection length, these cells retract against the applied suction pressure. However, retraction is only possible for suction pressures below ~1000 Pa (10,000 dyn/cm^2). In contrast to wild-type cells and talin-null mutants, both mutants deficient in myosin exhibit a drastically impaired retraction, even if the suction pressure is reduced to zero after aspiration.

5. Microfluorescence experiments strongly suggest that the retraction of enforced protrusions of wild-type cells is preceded by a redistribution of myosin II in the protrusion. The protein appears to accumulate in particular at the tip of the protrusion.

The finding of a threshold pressure for the onset of suction-enforced cellular protrusion shows that the process is associated with a mechanical instability of the cell envelope. In studies on other cell types, mechanisms like buckling (Evans, 1983) or membrane tension (Evans and Yeung, 1989) have been identified as the reason for similar instabilities. However, our findings indicate that in the present case the underlying process is of an irreversible nature, which is due mainly to the fracture of the bonds linking the plasma membrane and the cell body (cf. Discussion).

We therefore interpret the suction-enforced formation of cellular protrusions of *Dictyostelium* cells in terms of a quasiplastic deformation associated with the fracture of bonds between the cell envelope penetrating into the pipette and the cell body remaining behind. We present a theoretical model for this process and derive the relation between threshold pressure and bilayer cortex coupling strength.

The huge difference between the coupling strengths of wild-type cells and myosin II-deficient mutants indicates that, in addition to its importance for cell motility, myosin II also plays an important role in coupling between the cell envelope and the cell body.

MATERIALS AND METHODS

Mutant and wild-type AX2 cells of *Dictyostelium discoideum* were cultivated on SM agar plates, with *Klebsiella aerogenes* as a bacterial food source (Sussmann, 1966). Cells cultivated in axenic culture exhibited identical behavior. Three different mutants obtained by gene disruption were examined in this study. Mutants HG1666 and HS2205 failed to produce talin (Niewöhner et al., 1997) or the motor protein myosin II (Manstein et al., 1989), respectively. A third mutant was defective in the production of both talin and myosin II (HG1675; Eva Wallraff, unpublished). Two other mutant cell lines, containing a green fluorescent protein (mutant S65T) fused with monomeric actin (HG1662; Westphal et al., 1997) or myosin II (Moores et al., 1996), were used to study the spatial distribution of these proteins during aspiration. Immediately before the experiment, cells were taken from the edge of a colony and washed three times in cold 17 mM K-Na phosphate buffer (pH 6.0) to remove the bacteria. The washed cells were diluted to a density of ~10^3 ml^{-1} and injected into a measurement chamber (see below) containing the same buffer supplemented with 5 mg/ml bovine serum albumin (BSA) (Sigma, Deisenhofen, Germany), where they were allowed to attach to the substrate.

Setup

Our micropipette setup closely resembles systems described in the literature (Evans, 1989; Needham, 1993). Cells were observed in a chamber consisting of two parallel glass coverslips separated by a spacer of ~1 mm thickness. To allow easy access of the micropipette, the chamber was left open on two sides. Cylindrical glass micropipettes with an inner diameter of ~4 μm were prepared as described elsewhere (Evans, 1989) and connected to a micrometer-positioned water manometer, which allowed application of specified suction pressures that were measured by an in-line pressure transducer (DP15; Validyne, Northridge, CA). A micromanipulator (Narishige, Tokyo, Japan) was used to position the pipette. The chamber was mounted on the stage of an inverted microscope of the Zeiss Axiovert 135TV series (Carl Zeiss, Jena, Germany), equipped with differential interference contrast optics (DIC). The aspiration of single cells was observed with a 40× oil immersion objective (numerical aperture 1.3). Images were projected on the chip of a CCD camera (C2400-77; Hamamatsu, Hamamatsu City, Japan) and recorded on videotape. Recorded images were digitized with a Power Macintosh 9500 equipped with a frame grabber card (LG3; Scion Corp., Frederick, MD) and analyzed with the public domain software National Institutes of Health-image (version 1.6 by Wayne Rasband, National Institutes of Health, Bethesda, MD).

In the aspiration experiments a certain suction pressure, ranging from 100 to 2500 Pa, was preset. Than the pipette was moved gently against the leading or trailing edge of an adhering cell. We will argue below that the cells adhere only weakly with the central part and that therefore this does not affect the measurement of threshold pressures. Adhering cells were

used because they exhibit an obvious cell polarity, in contrast to nonadherent cells. With adherent cells we could easily distinguish between leading and trailing edges. In this context, "leading edge" refers to those areas of the cell circumference where pseudopods are formed, whereas "trailing edge" refers to the rest of the cell. Both parts of the cells were tested in our experiments.

RESULTS

Aspiration

The time course of a typical aspiration experiment is shown in Fig. 1. As soon as the pipette formed a tight seal with the cell membrane, the length of the aspirated cell portion increased within 2–5 s, depending on the suction pressure and the location on the cell, until an equilibrium length (projection length L_p) was reached. Details of the dynamics of aspiration will be addressed below. After aspiration, L_p remained constant for a period of ~10–20 s, after which an active response of the cell to the suction pressure became evident. In this third phase, wild-type cells managed to escape from the pipette if the suction pressure was less than ~1000 Pa. For suction pressures much higher than this value, an additional slower increase in the aspiration length could be observed.

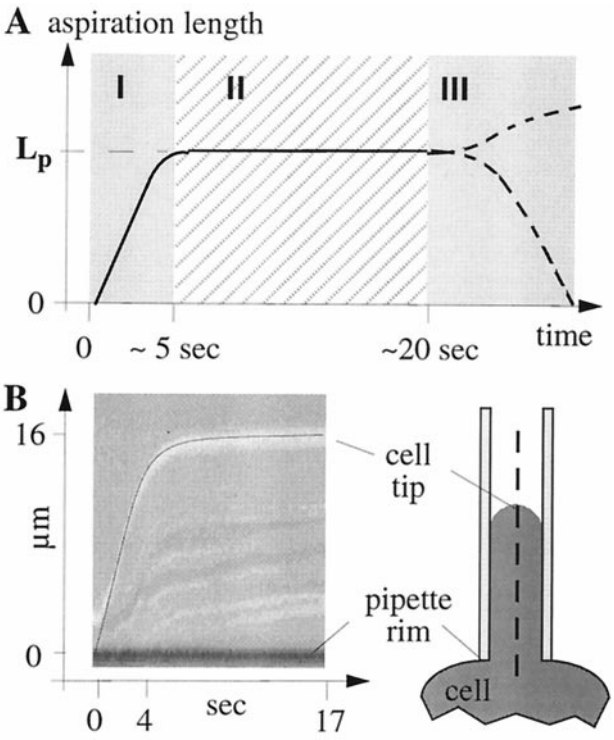

FIGURE 1 (*A*) Schematic of the typical time course of an aspiration experiment. The suction pressure is set before the pipette touches the cell membrane. If the suction pressure is high enough, the aspiration process starts immediately after a contact between membrane and pipette is formed. During this phase I the aspiration length L increases rapidly until the equilibrium length, L_p, is reached. During phase II this length remains unchanged while myosin II is redistributed within the cell. In phase III the cell starts to retract if the suction pressure does not exceed a critical value P_{crit}. For pressures above this value, the aspiration length increases again at a much slower rate. (*B*) A typical phase I as observed for wild-type cells is shown for comparison. The figure was created by plotting the intensities along the middle axis of the pipette during the aspiration experiment as successive vertical lines against the corresponding time. In the resulting image, the position of the tip of the aspirated cell lobe is marked by a thin black line. The rim of the pipette produces a horizontal black line. Obviously, the aspiration length grows approximately linearly in time during phase I.

It is important to note that aspiration did not permanently damage the cells. Usually less than 1 min after an aspirated cell had retracted from the pipette or had been expelled by reversing the pressure, the cell resumed its normal shape. No apparent changes in motility, size of contact area, or shape could be observed, even after aspirations at the highest suction pressures. Because cell motility is a very sensitive indicator for cell viability, no further tests of this parameter were performed.

To ensure that aspiration reflected the properties of native cells rather than changes induced by a previous aspiration experiment, cells were aspirated only once, or they were allowed to relax for several minutes between two aspirations. First and subsequent aspirations yielded identical results. This is in accord with the observation that cells relaxed within ~1 min after an aspiration expulsion cycle.

If the suction pressure was set to zero right after the onset of phase I, before an equilibrium length had been reached, the aspirated cell portion did not bounce back out of the pipette, as could be expected for buckling, but also passed through phase II and phase III. This observation supports the notion that aspiration initially causes irreversible deformations that are plastic rather than elastic in nature.

Threshold pressure and projection length

Fig. 2 shows the typical behavior of a wild-type cell, the leading and trailing edges of which have been exposed to the same suction pressure. The equilibrium projection length at the leading edge significantly exceeds the one obtained at the trailing edge of the cell.

Aspiration was only possible if the suction pressure exceeded a certain value, referred to as the threshold pressure, P_{th}. As is typical for experiments with single cells, this threshold pressure varied somewhat from cell to cell, although this variance was surprisingly small. For simplicity we defined the threshold pressure as that pressure at which more than 50% of the examined cells could be aspirated (Fig. 3).

Fig. 3 summarizes the results obtained for wild-type cells and mutants lacking talin. For wild type (Fig. 3, *A* and *B*), we observed significant differences in projection lengths and threshold pressures between leading and trailing edges. At the leading edge, a pressure of 200 ± 10 Pa sufficed to aspirate the cell, whereas a minimum pressure of 330 ± 20 Pa had to be applied to the trailing edge. Starting from these

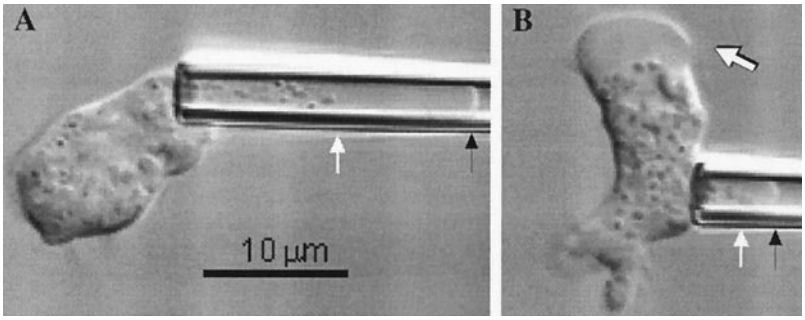

FIGURE 2 Behavior of cell front and end, when subjected to a suction pressure. The same suction pressure of 640 Pa has been applied to the front (*A*) and end (*B*) of a wild-type *Dictyostelium* cell. At the cell front, where a new pseudopod is forming, the aspiration length is significantly larger than at the trailing end of the cell. Black arrows denote the end of the aspirated cell lobe. Note that in both cases *A* and *B* the aspirated lobe exhibits a clear hyaline cap, free of internal cell compartments. The hyaline cap extends from the tip of the aspirated cell lobe to the beginning of the organelle-containing region (*thin white arrow*). The bold white arrow in *B* marks the pseudopod at the leading front of the cell.

pressures, the obtained projection length increased with the applied pressure. Talin-deficient cells (Fig. 3, *C* and *D*) also exhibited different projection lengths for leading and trailing edges. However, the threshold pressures appear to be the same for either side of talin mutants. We determined a value of 200 ± 10 Pa for the cell front and 230 ± 10 Pa for the cell end. These values are almost identical to the value obtained for the front of wild-type cells. Moreover, the projection lengths grew faster with suction pressure than for the wild-type cells.

Knockout of the motor protein myosin II had a dramatic effect on the threshold pressures P_{th}, which were about five

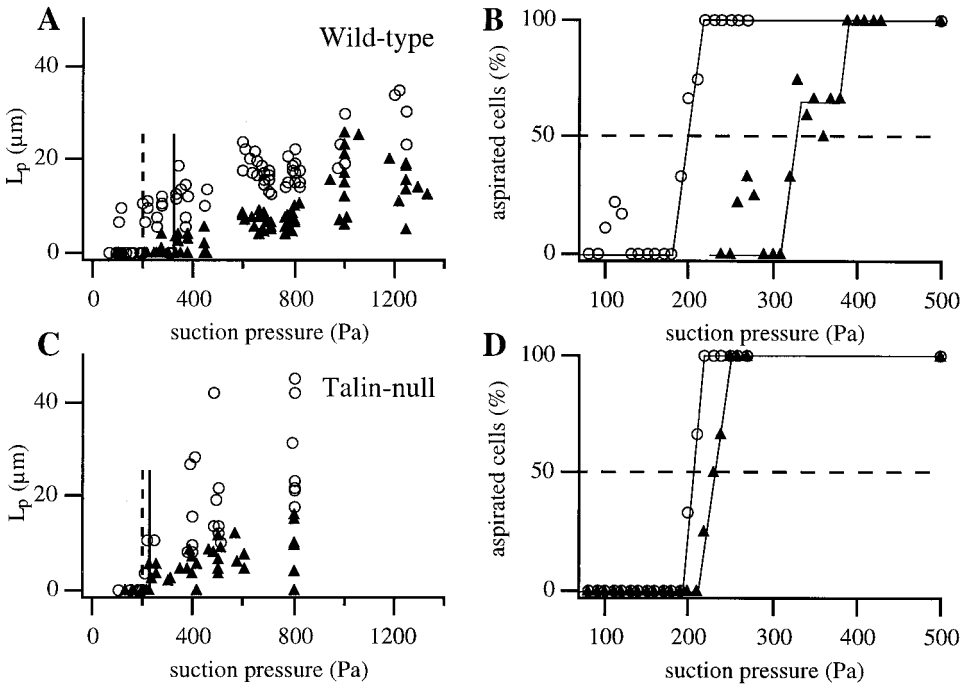

FIGURE 3 Aspiration experiments with wild-type cells and talin-null mutants. (*A*) The aspiration lengths as a function of the applied suction pressure for 140 wild-type cells. The same suction pressure yields significantly higher aspiration lengths at the cell front (○) as compared to the cell end (▲). The vertical lines denote the threshold pressures P_{th} that had to be overcome to aspirate the cell. P_{th} is defined as that pressure at which more than 50% of the cells could be aspirated. For better visibility, *B* shows the percentage of cells which could be aspirated in an interval of ±10 Pa around a given suction pressure. The dotted horizontal line denotes the 50% line. The threshold pressure at the leading front (*dashed line* in *A*) of ~200 Pa is much lower than the value obtained for the trailing end of ~330 Pa (*solid line* in *A*). (*C* and *D*) The corresponding graphs for 60 talin-null mutants. These mutants show the same qualitative behavior as the wild-type cells, while the absolute values of the projection lengths are somewhat higher. Note that the threshold pressure for the leading edge is ~200 Pa, which is the same value as that obtained for wild-type cells. At the trailing edge, however, knockout of talin significantly reduces P_{th} to ~230 Pa, which is approximately the same value as found for the leading edge.

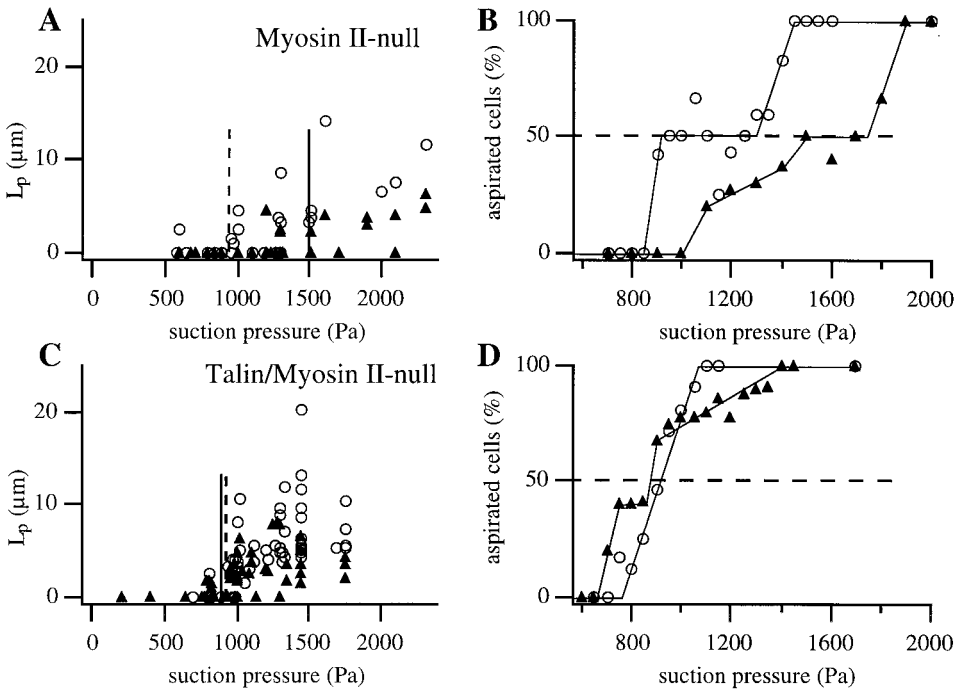

FIGURE 4 Aspiration experiments with myosin II-null mutants and double mutants, lacking both myosin II and talin. (*A*) The aspiration lengths as a function of the applied suction pressure for 40 myosin II-deficient cells. ○, Cell front; ▲, cell end. While these mutants exhibit the same qualitative difference between front and end, they appear to be much "harder" than wild-type cells. The threshold pressures are ~950 Pa for the cell front (*dashed vertical line*) and ~1500 Pa for the cell end (*solid line*). (*B*) Percentage of cells that could be aspirated in an interval of ±100 Pa around a given suction pressure. (*C* and *D*) Corresponding plots for 150 double mutants. As in Fig. 3, the knockout of talin does not significantly affect the threshold pressure at the leading edge, which is ~930 Pa for the double mutant. Moreover, P_{th} at the trailing edge is reduced to ~900 Pa, which is about the value found at the leading edge of the myosin II-null mutant.

times higher than for wild-type cells. In agreement with wild-type cells, however, the threshold pressure, P_{th}, at the leading edge was lower than the one obtained at the trailing edge. We determined a value of 950 ± 200 Pa at the leading edge and 1500 ± 200 Pa at the trailing edge (Fig. 4, *A* and *B*).

For the double mutant, lacking both talin and myosin II, we found a superposition of the defects caused by single mutations (Fig. 4, *C* and *D*). As with single mutants lacking talin, the threshold pressures were about the same at either side of the cells. In addition, these threshold pressures of ~930 Pa at the front and ~900 Pa at the cell end were as high as for the front of myosin II-deficient mutants.

Toward the end of phase II of an aspiration experiment, we frequently observed a sudden increase in the projection. While the projection length suddenly started growing again, usually increasing the projection length by a few micrometers, a structure remained visible at the old end position of the cell lobe (Fig. 5). Experiments with mutants containing GFP-labeled actin indicate a high concentration of actin in this structure. Moreover, its shape matches the original

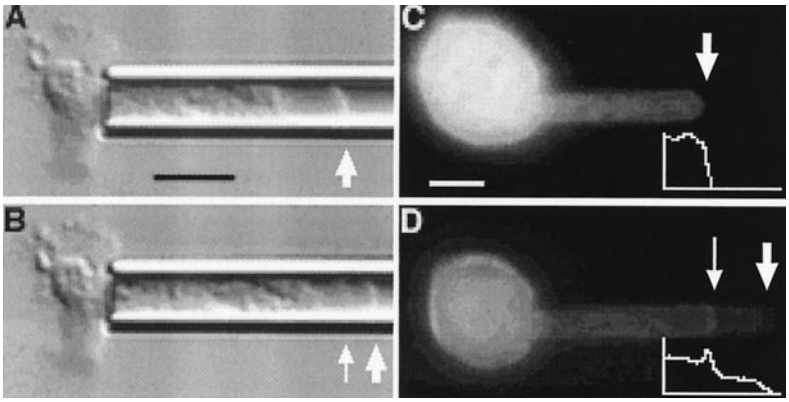

FIGURE 5 Decoupling of lipid bilayer and cortex during aspiration. Shown is an aspirated wild-type cell in DIC microscopy at the end of phase II, shortly before (*A*) and after (*B*) a sudden increase in the projection length. The wide arrow denotes the end position of the aspirated cell lobe. Note that in *B* a bright band remains visible (*thin arrow*) at the original end position of the lobe. The right column (*C* and *D*) shows the same process in fluorescence microscopy for a mutant cell containing GFP-labeled actin. Again wide arrows denote the end position of the aspirated cell lobe. Note the bright band (*thin arrow*) in *D*, which marks a high concentration of actin and corresponds well with the structure evident in *B*.

shape of the cell lobe at this position. These findings indicate that a thin cortical shell, which has formed in phase II beneath the lipid bilayer of the aspirated cell lobe, had been separated from the bilayer and was left behind as a result of the applied pressure. Such a decoupling of lipid bilayer and cortex could often be observed for both wild-type and talin-null mutants and far less frequently for cells lacking myosin II. The eventual retraction of cells from the pipette in phase III was not altered by such temporary decoupling events.

Retraction

After a period of constant aspiration length (phase II in Fig. 1), the aspirated cells tried to escape from the pipette in phase III. Wild-type cells could retract within 10–20 s, opposing suction pressures as high as 1000 Pa, which corresponds to a force of ~13 nN. Talin-deficient cells exhibited a reduced substrate adhesion and could only retract if the applied suction pressure was lower than ~600 Pa. Retraction started only after a redistribution of myosin II in the aspirated cell lobe had occurred. This could be observed in fluorescence experiments with mutants containing GFP-labeled myosin II (Fig. 6). Retraction clearly required the motor protein myosin II, because both the myosin II-null mutant and the double mutant, lacking both myosin II and talin, exhibited a markedly reduced retraction that lasted on the order of several minutes, even when the pressure was set to zero after aspiration.

It is interesting to compare the shapes of the aspirated cell part during aspiration and retraction. During retraction, the tip of the aspirated cell lobe forms ruffles and folds that appear to extend out of the cell body (Fig. 7), while a spherical cap can be observed in phase I during aspiration.

For pressures exceeding 1000 Pa for wild-type cells (600 Pa for talin-null mutants), the projection length gradually increased again in phase III. This process continued to a point where the part of the cell outside of the pipette had assumed an almost spherical shape. At this point, a further increase in the suction pressure always resulted in cell lysis. During this increase in L_p in phase III, we could frequently observe steplike increases in the projection length that coincided with the fusion of internal membranes like vacuoles with the outer cell membrane (Fig. 8).

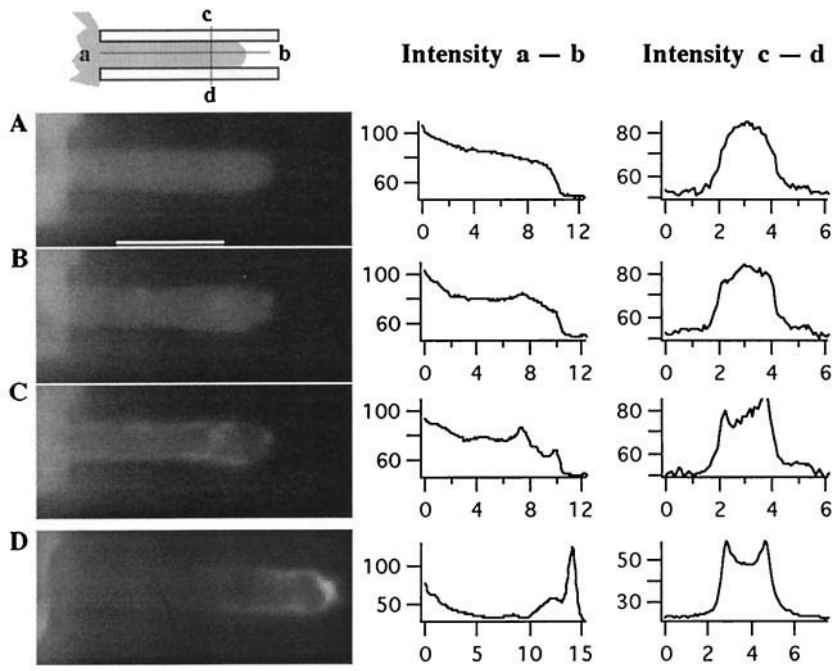

FIGURE 6 Redistribution of myosin II after aspiration precedes retraction. A mutant cell containing GFP-labeled myosin II was aspirated, and the fluorescence intensity in the aspirated cell lobe was observed over time. The left column shows fluorescence micrographs of the cell lobe, while the middle and right columns show the corresponding intensity distributions along and perpendicular to the pipette axes, respectively. The locations of the pixels used for intensity determination are shown in the sketch at the top of the figure. The line *a-b* is the center line of the pipette; the perpendicular line *c-d* intersects the cell protrusion 3–4 μm from the tip. Lengths are given in micrometers, and intensities as gray scale values ranging linearly from 0 (black) to 255 (white). (*A–C*) The same cell in intervals of 10 s, starting in *A* with the beginning of phase II (cf. Fig. 1). The white bar corresponds to 5 μm. High intensities correspond to high concentrations of myosin II. It is obvious that myosin II is accumulated along the wall of the pipette and in "hot spots" close to the tip of the aspirated cell lobe. Retraction starts after this redistribution is completed in *C*. For comparison, *D* shows the myosin II distribution for a different cell that has not been exposed to excitation light before, i.e., this cell was not stressed by the presence of photochemically generated radicals.

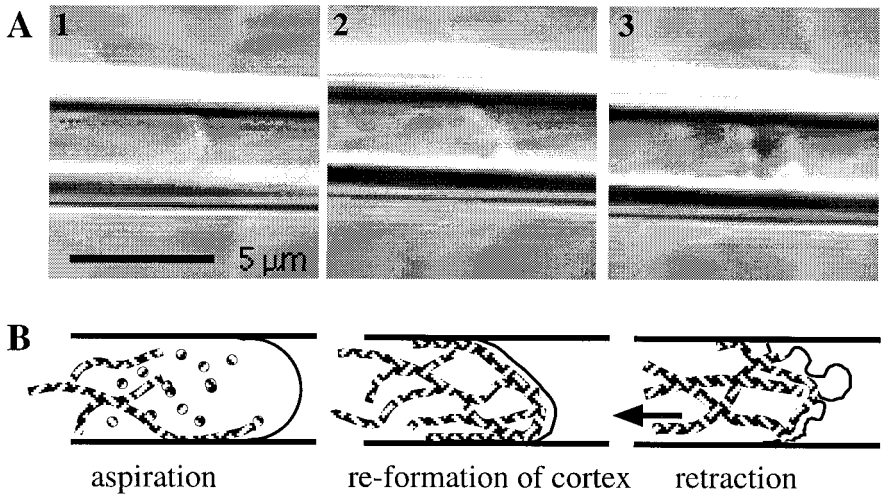

FIGURE 7 Shape changes reflect forces that act on the aspirated cell part. (*A*) DIC micrographs of the tip of an aspirated wild-type cell during phase I (*1*), at the beginning of phase II (*2*), and after an equilibrium projection length had been reached, and during retraction in phase III (*3*). (*B*) A model of the corresponding internal structure of the cell lobe. Note that in *1* the tip of the aspirated cell lobe forms a hemispherical cap because of the isotropic nature of the suction pressure driving the aspiration process. As soon as the aspiration length stops growing (*2*), the tip assumes an asymmetrical shape, possibly reflecting the formation of a new cortical shell and its coupling to the membrane. During retraction (*3*), the tip of the lobe becomes mechanically unstable, and one can observe the formation of ruffles and folds concomitant with myosin II aggregation. These findings suggest that contractile forces rather than osmotic pressure drive the retraction, and that these forces act on certain "spots" only where there is a high myosin II concentration.

DISCUSSION

The present micropipette aspiration experiments yield insight into the stability of the cell surface comprising the plasma membrane and the associated actin cortex, which is essential to many cellular functions such as locomotion (Cunningham et al., 1992). While the proteins involved in the coupling of membrane and cortex are well characterized biochemically, the physical coupling strength is just beginning to be studied (Shao and Hochmuth, 1996; Waugh and Bausermann, 1995; Hwang and Waugh, 1997). Because the pipette radius used, ~1.9 μm, is large compared to the mesh

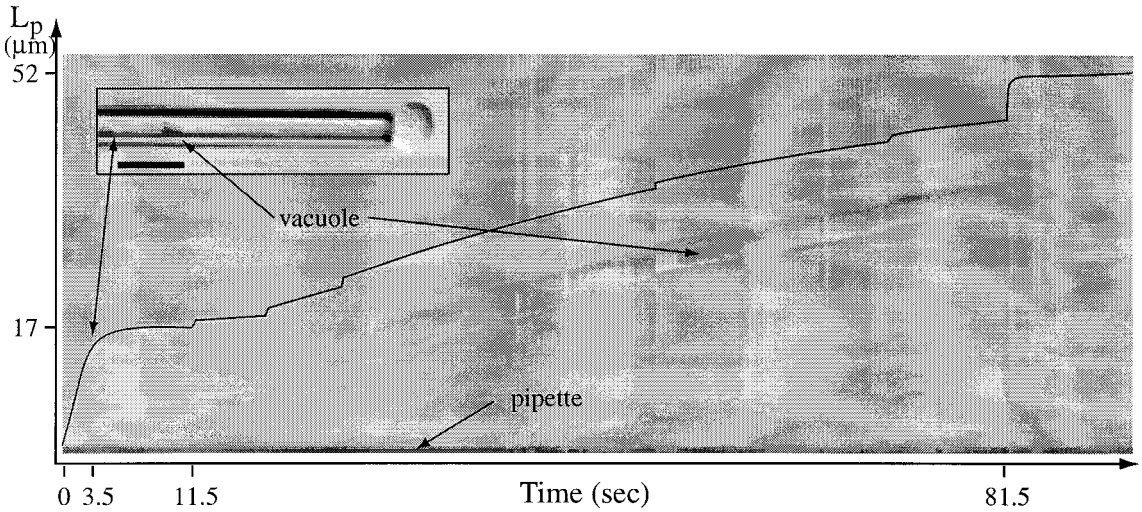

FIGURE 8 Fusion of internal membranes with the outer cell wall occurs at very high suction pressures where the cell is unable to retract. The insert shows an aspirated wild-type cell at a suction pressure of 1500 Pa. For every video frame of the recorded sequence, the intensity distribution along the middle axis of the pipette is plotted vertically on the graph (as in Fig. 1). The black line denotes the end position of the aspirated cell lobe in the pipette as a function of time. The initial rapid increase in L_p during the first 3.5 s (phase I) is followed by phase II, which lasts for another 8 s. Because of the high suction pressure the cell cannot retract, and the projection length gradually increases again in phase III. A vacuole that is visible in the aspirated cell lobe (see *inset*) until $t = 81.5$ s vanishes suddenly (*double arrow*). Simultaneously, the projection length increases by a length that corresponds exactly with the excess surface area created by fusion of the vacuole with the outer cell membrane.

size of the actin cortex, the membrane deformation was described by a continuum approach (cf. Appendix). Pipettes with significantly smaller radii (~1 μm) could not be used for aspiration because cell organelles blocked the entrance and aspirated cells tended to stick to these thin pipettes. Pipettes with a much larger radius (~3 μm) led to an aspiration of the whole cell. The present technique is different from tether pulling methods in which only a thin lipid membrane tether (radius ~25 nm) is pulled from the cell with the help of optical tweezers (Dai and Sheetz, 1995) or glass microcantilevers (Hwang and Waugh, 1997).

Quasiplastic deformation

The finding of a threshold pressure P_{th} for the aspiration of the cell into the pipette can only be explained by assuming that the initial step in aspiration is associated with a mechanical instability. There are various possible explanations: existence of a surface tension, buckling, unraveling of membrane folds, or fracture. The first case has been found by Evans and Yeung (1989) for granulocytes. Here aspiration occurred only above a critical suction pressure, $P_{crit} = 2\tau(1/R_p - 1/R_c)$, where τ is the persistent tension in the cell cortex, and R_p and R_c denote the radii of the suction pipette and the outer spherical segment of the cell, respectively. For a comparable pipette diameter $P_{crit} \approx 20$ Pa was found, which is an order of magnitude smaller than the values we found for wild-type cells. Buckling was observed during the initial aspiration step of erythrocytes (Evans, 1983). In our case, however, even at the beginning of phase I (Fig. 1), the aspirated cell part did not recoil immediately from the pipette when the suction pressure was removed. This excludes reversible deformations such as tension or buckling. The high velocity of aspiration (~10 μm/s), as well as the high suction pressure of several hundred Pa (corresponding to a force of several nN), suggests that the deformation is mainly due to a fracture between the membrane and the cortex. The fracture of specific bonds is a kinetic effect that depends strongly on the time scale of force application (Merkel et al., 1999). The rate of force application to the individual bonds linking membrane and cortex depends in a very complicated way on the stiffnesses and relaxation times of cell membrane, cortex, cytoplasm, and adhesion zone. (Another factor is the time it takes to form a seal between pipette and membrane. From our video recordings, we deduce an upper limit of 0.2 s for this time.) Because these material properties of the *Dictyostelium* cells and the exact location of the plane of fracture are not known, we adopted a quasistatic approach as the simplest model.

The exact plane of fracture is not known, but several lines of evidence indicate that the fracture occurs between the actin cortex and the lipid bilayer to which associated actin-binding proteins (such as talin and cortexilin), together with some actin, remain bound (cf. Fig. 9). First, the tip of an aspirated cell lobe forms a hyaline cap that is free of cell organelles, indicating that the actin cortex forms a barrier that keeps the organelles (at least initially) from entering the pipette. Second, a temporary separation of cortex and membrane could be seen in experiments with cells containing GFP-labeled actin (Fig. 5). In those cases where the projection length suddenly increases again at the end of phase II, a thin shell of actin at the original position of the tip of the aspirated lobe can be identified by both differential interference contrast microscopy and fluorescence microscopy. Third, the membrane-associated actin/myosin cortex forms rapidly at the freshly aspirated membrane (Fig. 6). The association of actin with the freshly aspirated membrane is further shown by the finding that the aspirated cell portion always exhibits pronounced GFP-actin fluorescence (cf. Fig. 5).

Detachment of the cell from the substrate is another process that could contribute, in principle, to the threshold behavior (Ra et al., 1999). However, we can exclude this

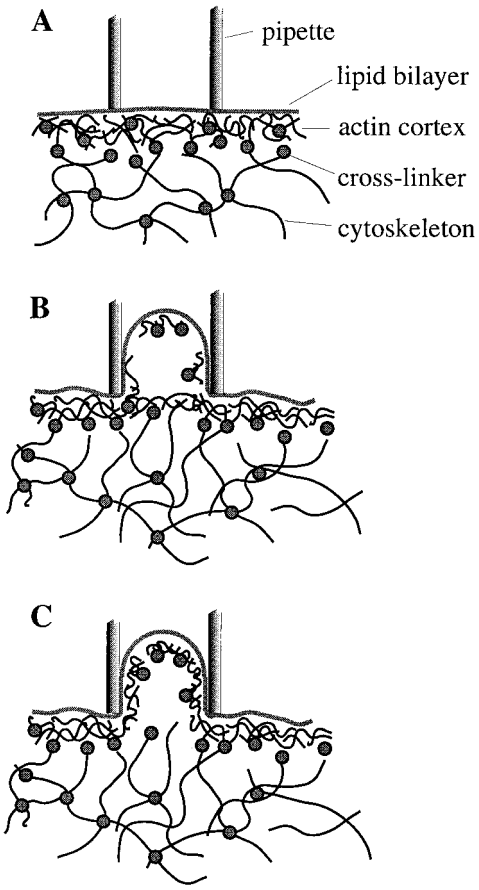

FIGURE 9 (A) Schematic of the first step in an aspiration experiment, the formation of a tight seal between pipette and plasma membrane. (*B*) If the suction pressure exceeds the threshold value P_{th}, a fracture is assumed to occur between lipid bilayer and the underlying actin cortex, including a partial disruption of the latter. The exact plane of the fracture is not known. (*C*) Another possibility, in which most of the cortex is aspirated together with the bilayer.

possibility because the contact areas did not change at all at the onset of aspiration. This was tested by reflection interference contrast microscopy, as described by Schindl et al. (1995).

Deformations that are based on fractures but preserve the structure of the deformed body are usually called plastic deformations. In our case, the composite membrane is temporarily disrupted but is reestablished during the aspiration experiment. We therefore describe the underlying process of deformation as "quasiplastic."

Evaluation of coupling strength σ from elongation-pressure curves

To determine the coupling strength between cell membrane and cortex, we used a model as depicted in Fig. 9, in which a two-dimensional array of bonds accounts for the interaction between cortex (assumed to be a rigid body) and membrane (modeled as an elastic plate). The membrane-cortex interaction is characterized by a coupling constant σ, which is the energy per unit area required to fracture the bonds (cf. Fig. 10). In the Appendix a relationship between the threshold pressure P_{th} and the coupling constant σ is established, which can be used to estimate the coupling strength. The pipette rim is kept close to the outer surface of the membrane, forming a tight seal between pipette and membrane. Under the influence of a suction pressure, the composite shell (i.e., membrane and cortex) is initially deformed as a whole. As soon as the energy release W associated with the membrane deformation matches the energy required for breaking the bonds, fracture occurs and the cell is aspirated into the pipette.

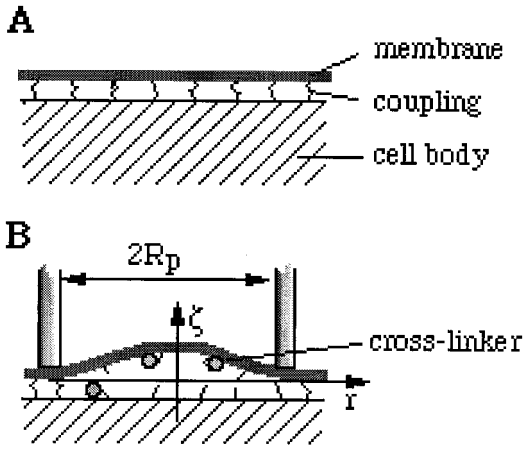

FIGURE 10 Model for the theoretical description of the threshold pressure. The cell is assumed to consist of the composite membrane and the underlying cell body. Aspiration starts if the applied suction pressure is high enough to break the bonds between cell body and membrane. After fracture some actin binding proteins (e.g., talin, cortexillin, and α-actinin) remain at the membrane.

The deformation of the composite membrane depends both on the membrane's bending modulus κ and on its surface tension γ. In the Appendix we deduce the condition of fracture for two limiting cases: bending and tension-dominated deformation (Eqs. 10 and 11, respectively). Because the effective values of the membrane bending modulus and the tension depend on the position of the plane of fracture, which is not known, we consider below two realistic limiting cases.

1. Only the bilayer is peeled from the cortex. For the following reason, this case corresponds to talin-deficient cells. The bending modulus of lipid vesicles is on the order of 10^{-19} J, and the membrane tension for flaccid vesicles is $\sim 10^{-7}$ N/m (Duwe et al., 1987; Bo and Waugh, 1989; Evans and Rawicz, 1990; Mutz and Helfrich, 1990). These values agree rather well with the values $\kappa = 3 \times 10^{-19}$ J and $\gamma = 1$ μN/m found previously for talin-null *Dictyostelium* cells (Simson et al., 1998).

2. The whole composite shell is aspirated. In this case the bending stiffness and the membrane tension are expected to be about two orders of magnitude larger. For wild-type *Dictyostelium* cells, values of $\gamma \approx 3 \times 10^{-6}$ N/m and $\kappa \approx 400 k_B T \approx 2 \times 10^{-18}$ J were found (Simson et al., 1998). For comparison, the tension of white blood cells is $\gamma \approx 3 \times 10^{-5}$ N/m (Evans and Yeung, 1989; Lelièvre et al., 1995).

In both limiting cases, the contributions of bending and tension to the deformation energy are comparable (or $\gamma R_p^2/\kappa \approx 1$, where R_p denotes the pipette radius). Therefore, Eq. 9 (Appendix) has to be used to estimate the coupling constant σ. Table 1 lists the values of σ, obtained for the cell front and end of wild-type cells and talin-null mutants, for the two limiting cases described above. Here we used the values of κ and γ determined in our previous study (Simson et al., 1998). Because in reality fracture occurs probably within the cortex (Fig. 9 *B*), the actual value of σ should lie somewhere between the limiting values given in Table 1. Because for the myosin-null mutants κ and γ are not known, we refrained from including the respective data in Table 1.

TABLE 1 Coupling constants for the front and rear ends of *Dictyostelium* cells, as obtained by evaluation of the threshold pressure for aspiration (Eq. 9)

		σ (mJ/m^2)	
	P_{th} (Pa)	(a) Lipid membrane	(b) Membrane + cortex
Wild-type (AX2)			
Cell front	200	4	0.6
Cell end	330	11	1.6
Talin-null (HG1666)			
Cell front	200	4	—
Cell end	200	4	—

Shown are the results for two limiting cases: (a) only the lipid membrane is peeled away from the cortex ($\kappa \approx 10^{-19}$ J), and (b) the composite shell remains intact during aspiration ($\kappa \approx 1.6 \times 10^{-18}$ J). For the talin-null mutant cells case b is highly unlikely and therefore is not included. The pipette radius was 1.9 μm.

According to Table 1, the values for σ range from ~0.6 mJ/m^2 to ~4 mJ/m^2 for the cell front and from ~1.6 mJ/m^2 to ~11 mJ/m^2 for the trailing end. The coupling strength at the cell end is always by about an order of magnitude higher than at the cell front, because of the lower threshold pressure found in this latter region.

A remarkable finding is the difference between the coupling constants at the leading front and at the trailing end of wild-type cells and the absence of this difference for talin-deficient cells. This provides evidence that the coupling of the actin cortex to the membrane is weaker at the front of pseudopods.

It is interesting to estimate the Young's modulus and the bending modulus of the actin cortex, which exhibits a thickness on the order of ~0.2 μm. According to Podolski and Steck (1990), the cortical F-actin concentration is $c_A \approx 30$ μM (calculated for the whole cell volume of 1000 μm^3), and the average filament length is $L \approx 0.25$ μm. Rheological studies of actin networks in vitro show that a fully cross-linked actin network of $c_A \approx 10$ μM exhibits a shear modulus and thus a Young's modulus of $E \approx 5$ Pa (Tempel et al., 1996). Because the elastic modulus scales with the F-actin concentration as $E \propto {c_A}^{5/2}$ (MacKintosh et al., 1995), one estimates a Young's modulus of the cortex of *Dictyostelium* cells of $E \approx 3 \times 10^4$ Pa. This corresponds to a bending stiffness of $\kappa \approx 2 \times 10^{-17}$ J or $5000 k_B T$. This exceeds the bending stiffness of $\kappa \approx 400 k_B T$ found previously for wild-type cells (Simson et al., 1998) by an order of magnitude. However, the above estimate is an upper limit of the Young's modulus and would hold if all points of entanglement of F-actin were cross-linked. We expect the abundant presence of cortical defects in living cells that would explain their reduced bending stiffness.

With respect to our conclusions about the membrane-cortex coupling in *Dictyostelium* cells, the findings of Schütz and Keller (1998) on colchicine-treated Walker carcinosarcoma cells are notable. These cells are highly mobile and move by blebbing at the leading edge. Schütz and Keller found that micropipette aspiration of these cells resulted in bleb formation. In all cases, these blebs formed at the leading edge of the cells, irrespective of the site of aspiration (leading or trailing edge). This finding clearly indicates that cortex and membrane are partially decoupled at the leading edge of these cells.

Knockout of myosin II significantly increases the stability of the composite membrane against disruption

An intriguing result is the drastic increase of the threshold pressure and thus of the stability (or σ) of the cell envelope after the removal of myosin II. For the assumption that the lipid bilayer is peeled away from the membrane during aspiration, myosin-deficient cells exhibit a value of $\sigma \approx 100$ mJ/m^2 for the front and $\sigma \approx 250$ mJ/m^2 for the rear end. A comparable increase in σ was observed for the double mutants lacking both talin and myosin II. As in talin-deficient mutants, no significant difference between the front and rear ends of the double mutants was observed. Our findings suggest that myosin II plays an important role in the dynamic softening of the actin cortex during deformation. (The motor activity of randomly oriented myosin results in an enhanced random transport of material. Thus actin networks appear to be softer if they are subject to myosin action.) Myosin II is an active cross-linker that can associate and dissociate very rapidly in the presence of ATP, and the myosin II-induced softening is thus expected to be a dynamic property (Prassler et al., 1997). Another possible explanation is that knockout of myosin II is compensated for by an overabundance of other cross-linkers, forming stronger bonds than myosin II, thus leading to the observed increase in P_{th} and σ.

It is important to note the remarkable difference between our study and measurements of the deformability of *Dictyostelium* cells by cell poking (Pasternak et al., 1989). When small indentations (~0.5 μm) of the cell membrane caused by a glass stylus of 1.5-μm diameter were analyzed, a 30% decrease in the stiffness of AX4 *Dictyostelium* cells after knockout of myosin II was reported. This appears to be in contradiction to our findings of a drastically increased stability of myosin II mutants derived from the AX2 *Dictyostelium* strain (Moores et al., 1996). Provided the AX4 and AX2 strains of *Dictyostelium discoideum* do not exhibit intrinsically different properties, this apparent contradiction can be attributed to the different modes of deformation employed. First, poking and aspiration deform the membrane in different directions. Second, the response of the cell to these deformations is elastic in the case of poking and plastic for aspiration. While the underlying molecular mechanism remains obscure, the same biochemical change (knockout of myosin II) appears to facilitate an elastic indentation of the membrane, while it increases the stability of the composite membrane with respect to plastic deformation.

Reformation of a new cortex precedes retraction

After aspiration of a cell lobe into the pipette, the cell tries to retract this enforced protrusion. Please note that cell retraction appears to be a key step in the locomotion of *Dictyostelium* cells (Jay et al., 1995). The present technique enables us to study the internal processes preceding retraction. According to Fig. 6, restoration of a cortex, which is essential to the retraction of the advanced lobe, lasts for ~20 s. During this period (which corresponds to phase II) myosin II is accumulated in the aspirated cell part, and retraction starts only after this redistribution has been achieved. Myosin II is not distributed evenly in the lobe but appears to be accumulated at certain "hot spots" (cf. Fig. 6), presumably where the contractile force is generated during retraction. These results agree with studies on the in vivo

dynamics of myosin II, which also revealed discrete actin-rich and myosin II-rich structures at the posterior ends of *Dictyostelium* cells (Yumura et al., 1984; Chu and Fukui, 1996; Moores et al., 1996).

Mutants lacking myosin II were unable to retract, even at the lowest suction pressures. Because these mutants exhibit a significantly impaired motility (Jay et al., 1995; Wessels et al., 1988), this finding suggests that retraction is an essential driving force for cell crawling.

The restoration of the membrane-associated cytoskeleton in phase II is also revealed by the shape changes in the tip of the aspirated cell lobe. The tip is shaped spherically during aspiration (Fig. 7 *A1*), reflecting the isotropic pressure, but becomes asymmetrical as soon as the projection stops growing (Fig. 7 *A2*). This finding can be attributed to the onset of the formation of a new cortex and its coupling to the lipid bilayer. During the following retraction in phase III, the tip forms ruffles and small blebs (Fig. 7 *A3*). The uneven distribution of myosin II in the cell lobe (Fig. 6) suggests that the contractile forces act at certain points only. A similar restoration of an actin cortex after termination of the protrusion can also be observed in those instances where the projection length suddenly increases again at the end of phase II (Fig. 5). Here a new actin cortex has been formed during phase II that is separated from the bilayer and stays at the original position of the tip of the aspirated cell lobe.

Two observations suggest that aspiration and subsequent cell retraction caused a reversal of the cell polarity if the leading edge had been aspirated. First, after retraction, all cells moved away from the pipette. Second, the newly formed trailing end exhibited the same elevated threshold pressure as the trailing edge of an undisturbed cell as was found by testing by immediate reaspiration after cell retraction.

Fusion of internal cell compartments with the composite membrane creates excess surface area

Retraction of protrusions from the pipette was impossible if the suction pressure exceeded a certain value, which was ~1000 Pa for wild-type cells and ~600 Pa for talin-null mutants. For pressures above these values, the projection length increased again with the onset of phase III, but with considerably slower speed than during the initial aspiration in phase I. The aspirated cylindrical cell lobe requires more surface area per unit volume than the approximately spherically shaped part of the cell outside of the pipette. A further increase in the projection length therefore requires a reservoir of excess area. The projection length will therefore cease growing if the available excess area has been used up. Evidence for this view is provided by our aspiration experiments at very high suction pressures, where fusion of internal cell vacuoles or vesicles with the outer cell membrane is observed through stepwise increases in the projection length (Fig. 8).

Our experiments indicate that the motility of *Dictyostelium* cells correlates with a global cell polarity, which manifests itself in a "soft" leading edge, characterized by a low aspiration threshold pressure and large projection lengths, and a comparatively "stiff" trailing edge, characterized by a high threshold pressure and low projection lengths. The difference between these regions appears to be due at least in part to the action of talin, which mediates the coupling of lipid bilayer and the underlying cytoskeleton. It is more likely due, however, to a much thinner and possibly less strongly cross-linked actin cortex at the front of pseudopodia, inasmuch as removal of talin does not appreciably affect the threshold pressure at the leading front. Our experiments also stress the dual role of talin, which can act as an actin-membrane linker and as a nucleator of actin polymerization at the leading front of pseudopods. The cell polarity can be reversed, as is shown by our retraction experiments. Regardless of whether the cell had initially been aspirated at its front or at its end, the aspirated cell part always transformed into a cell end.

APPENDIX: STATIC APPROACH TO THE DESCRIPTION OF SPLITTING THE CELL MEMBRANE FROM THE CELL BODY

We consider a membrane coupled to the cell body by a two-dimensional array of bonds (Fig. 10). The membrane can be either a single lipid bilayer or a bilayer with some adsorbed F-actin. If the interbond distance is much smaller than the pipette radius, a continuous approach is valid. In this case the coupling strength between the cell body and the membrane is described by the parameter σ, which is a measure of a work per unit area needed to break the bonds. In the present calculation we assume the cell body to be rigid. Because in reality the cell body is elastic, this simplification leads to an overestimation of the coupling constant σ. We consider the part of the membrane under the pipette as a thin elastic plate with bending modulus κ and lateral tension γ. Consider the situation displayed in Fig. 10 *B*, where all of the bonds between membrane and cortex in the circular area under the pipette are broken. The equation of equilibrium for a flat membrane under tension can be obtained from the general expression established for the membrane of a spherical cell with radius R_c (Boulbitch 1998). In the limit of $R_c \to \infty$ this expression makes it possible to obtain the free energy F of a flat membrane. Subtracting from the latter the work $\int\int P\zeta \, \mathrm{dA}$ associated with the deformation, one finds the release of elastic energy:

$$W = F - \int\int P\zeta \, \mathrm{d}A = \int\int \left\{ \frac{1}{2}(\kappa\zeta\Delta^2\zeta - \gamma\zeta\Delta\zeta) - P\zeta \right\} \mathrm{d}A, \tag{1}$$

where ζ is the displacement normal to the plane of the undeformed membrane, Δ is the Laplace operator, and the integration is performed over the circular area A under the pipette. Variation of the energy equation (Eq. 1) with respect to the displacement ζ yields the equation of state,

$$\kappa\Delta^2\zeta - \gamma\Delta\zeta = P. \tag{2}$$

Substituting $\Psi = \Delta\zeta$ in Eq. 2, one obtains the equation

$$\kappa\Delta\Psi - \gamma\Psi = P, \tag{3}$$

which has the general solution

$$\Psi = -\frac{P}{\gamma} + C_1 I_0\left(r\sqrt{\frac{\gamma}{\kappa}}\right) + C_2 K_0\left(r\sqrt{\frac{\gamma}{\kappa}}\right), \quad (4)$$

where I_0 and K_0 are modified Bessel functions of order zero, and C_1 and C_2 are arbitrary constants. According to the geometry of the experiment, we look for a cylindrically symmetrical solution of Eq. 2. Using the representation $\Psi = \Delta\zeta = r - 1(r\zeta')'$ (where $\zeta' \equiv d\zeta/dr$) and performing the integration, one finds a general solution of Eq. 2 that has the form

$$\zeta = -\frac{P}{4\gamma} r^2 + C_1 I_0\left(r\sqrt{\frac{\gamma}{\kappa}}\right) + C_2 K_0\left(r\sqrt{\frac{\gamma}{\kappa}}\right) + C_3 \ln r + C_4, \quad (5)$$

where C_3 and C_4 are again arbitrary constants.

The boundary conditions corresponding to our experimental geometry can be expressed as $\zeta = 0$, $\partial\zeta/\partial r = 0$ at $r = R_p$. The first condition describes the fact that the membrane edge undergoes no vertical displacement at the rim of the pipette ($r = R_p$), whereas the second condition ensures that the membrane remains smooth. Because there is no singularity in the origin of the coordinates (i.e., no localized force is applied; cf. Landau and Lifshitz, 1959), one should take $C_2 = C_3 = 0$. The solution, satisfying the above boundary conditions, has the form

$$\zeta = \frac{P}{4\gamma}\left\{2R_p\sqrt{\frac{\kappa}{\gamma}}\frac{I_0(r\sqrt{\gamma/\kappa}) - I_0(R_p\sqrt{\gamma/\kappa})}{I_1(R_p\sqrt{\gamma/\kappa})} + R_p^2 - r^2\right\}. \quad (6)$$

Substitution of Eq. 2 into the expression for the energy release (Eq. 1) yields a simple representation for W:

$$W = -\frac{P}{2}\int\int \zeta \, dA. \quad (7)$$

With this and Eq. 6, we obtain

$$W = -\frac{\pi P^2 R_p^4}{16\gamma}\left\{\frac{8\kappa}{\gamma R_p^2} + 1 - 4\sqrt{\frac{\kappa}{\gamma R_p^2}}\frac{I_0(\sqrt{\gamma R_p^2/\kappa})}{I_1(\sqrt{\gamma R_p^2/\kappa})}\right\}. \quad (8)$$

As soon as the threshold pressure P_{th} is reached, the energy release during bending equals the energy required for fracturing bonds, and a splitting of cell membrane and cell body occurs. Therefore, the condition of fracture takes the form $W + \pi R_p^2\sigma = 0$, or

$$\sigma = \frac{P_{th}^2 R_p^2}{16\gamma}\left\{\frac{8\kappa}{\gamma R_p^2} + 1 - 4\sqrt{\frac{\kappa}{\gamma R_p^2}}\frac{I_0(\sqrt{\gamma R_p^2/\kappa})}{I_1(\sqrt{\gamma R_p^2/\kappa})}\right\}. \quad (9)$$

Consider two limiting regimes. If the bending energy $F_b = \frac{1}{2}\kappa\int\int\zeta\Delta^2\zeta \, dA \approx \kappa\zeta^2/R_p^2$ is much smaller than the tension energy $F_t = \frac{1}{2}\gamma\int(\nabla\zeta)^2 \approx \gamma\zeta^2$, that is, if $1 \ll \gamma R_p^2/\kappa$, one finds the tension-dominated regime. In this limit, we have $I_0(\sqrt{\gamma R_p^2/\kappa}) \approx I_1(\sqrt{\gamma R_p^2/\kappa}) \approx \exp\{\sqrt{\gamma R_p^2/\kappa}\}(2\pi\gamma R_p^2/\kappa)^{-1/2}$. The energy release and the condition of fracture then have the form

$$W = -\frac{\pi P^2 R_p^4}{16\gamma}; \quad \sigma = \frac{P^2 R_p^2}{16\gamma}. \quad (10)$$

In the bending-dominated regime, $\gamma R_p^2/\kappa \ll 1$, an expansion of the Bessel functions into a power series yields

$$W = -\frac{\pi P^2 R_p^6}{384\kappa}; \quad \sigma = \frac{P^2 R_p^4}{384\kappa}. \quad (11)$$

We thank Prof. James A. Spudich (Stanford) for providing the GFP-myosin II mutants. Prof. Schleicher (Munich) kindly gave us some of the wild-type cells. We are indebted to Dr. Günther Gerisch (Martinsried) for generously providing us with all of the other cells and for many helpful discussions and advice.

This work was supported by the Alexander von Humboldt Foundation and by the Deutsche Forschungsgemeinschaft, via grant SA246/28-1 and the group grant SFB 266.

REFERENCES

Bo, L., and R. F. Waugh. 1989. Determination of bilayer membrane bending stiffness by tether formation from giant, thin-walled vesicles. *Biophys. J.* 55:509–517.

Boulbitch, A. 1998. Deflection of a cell membrane under application of a local force. *Phys. Rev. E.* 57:2123–2128.

Bray, D., and J. G. White. 1988. Cortical flow in animal cells. *Science.* 239:883–888.

Bruinsma, R. 1996. Physical aspects of adhesion of leukocytes. *In* Physics of Biomaterials: Fluctuations, Self-Assembly, and Evolution. T. Riste and D. Sherrington, editors. Kluwer Academic Publishers, Amsterdam. 61–75.

Chu, Q., and Y. Fukui. 1996. In vivo dynamics of myosin II in *Dictyostelium* by fluorescent analogue cytochemistry. *Cell Motil. Cytoskeleton.* 35:254–268.

Condeelis, J. 1993a. Life at the leading edge: the formation of cell protrusions. *Annu. Rev. Cell Biol.* 9:411–414.

Condeelis, J. 1993b. Understanding the cortex of crawling cells: insights from *Dictyostelium. Trends Cell Biol.* 3:371–376.

Cunningham, C. C. 1995. Actin polymerization and intracellular solvent flow in cell surface blebbing. *J. Cell Biol.* 129:1589–1599.

Cunningham, C. C., J. B. Gorlin, D. J. Kwiatkowski, J. H. Hartwig, P. A. Janmey, H. R. Byers, and T. P. Stossel. 1992. Actin-binding protein requirement for cortical stability and efficient locomotion. *Science.* 255:325–327.

Dai, J., and M. Sheetz. 1995. Mechanical properties of neuronal growth cone membrane studied by tether formation with laser optical tweezers. *Biophys. J.* 68:988–996.

Duwe, H. P., H. Engelhardt, A. Zilker, and E. Sackmann. 1987. Curvature elasticity of smectic A lipid bilayers and cell plasma membranes. *Mol. Cryst. Liq. Cryst.* 152:1–7.

Evans, E. A. 1983. Bending elastic modulus of red blood cell membrane derived from buckling instability in micropipet aspiration tests. *Biophys. J.* 43:27–30.

Evans, E. A. 1989. Structure and deformation properties of red blood cells: concepts and quantitative methods. *Methods Enzymol.* 173:3–35.

Evans, E. 1995. Physical actions in biological adhesion. *In* Handbook of Biological Physics 1B. R. Lipowsky and E. Sackmann, editors. North Holland, Amsterdam. 723–754.

Evans, E., and W. Rawicz. 1990. Entropy-driven tension and bending elasticity in condensed-fluid membranes. *Phys. Rev. Lett.* 64: 2094–2097.

Evans, E., and A. Yeung. 1989. Apparent viscosity and cortical tension of blood granulocyte determined by micropipet aspiration. *Biophys. J.* 56:151–160.

Horwitz, A., K. Duggan, C. Buck, M. C. Beckerle, and K. Burridge. 1986. Interaction of plasma membrane fibronectin receptor with talin—a transmembrane linkage. *Nature.* 320:531–533.

Hwang, W. C., and R. E. Waugh. 1997. Energy of dissociation of lipid bilayer from the membrane skeleton of red blood cells. *Biophys. J.* 72:2669–2678.

Isenberg, G., and V. Niggli. 1998. Interaction of cytoskeletal proteins with membrane lipids. *Int. Rev. Cytol.* 178:73–125.

Jay, P. Y., P. A. Pham, S. A. Wong, and E. Elson. 1995. A mechanical function of myosin II in cell motility. *Cell Sci.* 108:387–393.

Landau, L. D., and E. M. Lifshitz. 1959. Theory of Elasticity. Pergamon Press, Elmsford, NY.

Lelièvre, J. C., C. Bucherer, S. Geiger, C. Lacombe, and V. Vereycken. 1995. Blood cell biomechanics evaluated by the single-cell micromanipulation. *J. Phys. III France.* 5:1689–1705.

MacKintosh, F. C., J. Käs, and P. A. Janmey. 1995. Elasticity of semiflexible biopolymer networks. *Phys. Rev. Lett.* 75:4425–4428.

Manstein, D. J., M. A. Titus, A. DeLozanne, and J. A. Spudich. 1989. Gene replacement in *Dictyostelium*: generation of myosin null mutants. *EMBO J.* 8:923–932.

Merkel, R., P. Nassoy, A. Leung, K. Ritchie, and E. Evans. 1999. Energy landscapes of receptor-ligand bonds explored with dynamic force spectroscopy. *Nature.* 397:50–53.

Moores, S. L., J. H. Sabry, and J. A. Spudich. 1996. Myosin dynamics in live *Dictyostelium* cells. *Proc. Natl. Acad. Sci. USA.* 93:443–446.

Mutz, M., and W. Helfrich. 1990. Bending rigidities of some biological model membranes as obtained from the Fourier analysis of contour sections. *J. Phys. France.* 51:991–1002.

Needham, D. 1993. Measurement of interbilayer adhesion energies. *Methods Enzymol.* 220:111–130.

Niewöhner, J., I. Weber, M. Maniak, A. Müller-Taubenberger, and G. Gerisch. 1997. Talin-null cells of *Dictyostelium* are strongly defective in adhesion to particle and substrate surfaces and slightly impaired in cytokinesis. *J. Cell Biol.* 138:349–361.

Oster, G. F., and A. S. Perelson. 1987. The physics of cell motility. *J. Cell Sci. Suppl.* 8:35–54.

Pasternak, C., J. A. Spudich, and E. L. Elson. 1989. Capping of surface receptors and concomitant cortical tension are generated by conventional myosin. *Nature.* 341:549–551.

Podolski, J. L., and T. L. Steck. 1990. Length distribution of F-actin in *Dictyostelium discoideum. J. Biol. Chem.* 265:1312–1318.

Prassler, J., S. Stocker, G. Marriott, M. Heidecker, J. Kellermann, and G. Gerisch. 1997. Interaction of a *Dictyostelium* member of the plastin/fimbrin family with actin filaments and actin-myosin complexes. *Mol. Biol. Cell.* 8:83–95.

Ra, H. J., C. Picart, H. Feng, H. L. Sweeney, and D. E. Discher. 1999. Muscle cell peeling from micropatterned collagen: direct probing of focal and molecular properties of matrix adhesion. *J. Cell Sci.* 112: 1425–1436.

Sackmann, E. 1995. Physical basis of self-organization and function of membranes: Physics of vesicles. *In* Structure and Dynamics of Membranes, Vol. IA. R. Lipowsky and E. Sackmann, editors. Elsevier/North Holland, Amsterdam. 213–304.

Schindl, M., E. Wallraff, B. Deubzer, W. Witke, G. Gerisch, and E. Sackmann. 1995. Cell-substrate interactions and locomotion of *Dictyostelium* wild-type and mutants defective in three cytoskeletal proteins: a study using quantitative reflection interference contrast microscopy. *Biophys. J.* 68:1177–1190.

Schütz, K., and H. Keller. 1998. Protrusion, contraction and segregation of membrane components associated with passive deformation and shape recovery of Walker carcinosarcoma cells. *Eur. J. Cell Biol.* 77:100–110.

Seifert, U., and R. Lipowsky. 1990. Adhesion of vesicles. *Phys. Rev. A.* 42:4768–4771.

Shao, J., and R. Hochmuth. 1996. Micropipette suction for measuring piconewton forces of adhesion and tether formation from neutrophil membranes. *Biophys. J.* 71:2892–2901.

Simson, R., A. Albersdörfer, and E. Sackmann. 1997. Adhesion of soft biological shells controlled by bending elasticity and macromolecular networks. *In* Statistical Mechanics in Physics and Biology. D. Wirtz and T. C. Halsey, editors. Materials Research Society, Warrendale, PA. 3–13.

Simson, R., E. Wallraff, J. Faix, J. Niewöhner, G. Gerisch, and E. Sackmann. 1998. Membrane bending modulus and adhesion energy of wild-type and mutant cells of *Dictyostelium* lacking talin or cortexillins. *Biophys. J.* 74:514–522.

Sussmann, M. 1966. Biochemical and genetic methods in the study of cellular slime mold development. *Methods Cell Physiol.* 2:397–410.

Tempel, M., G. Isenberg, and E. Sackmann. 1996. Temperature-induced sol-gel transition and microgel formation in α-actinin cross-linked actin networks: a rheological study. *Phys. Rev. E.* 54:1802–1810.

Waugh, R., and R. Bausermann. 1995. Physical measurements of bilayer-skeletal separation forces. *Ann. Biomed. Eng.* 23:308–321.

Wessels, D., D. R. Soll, D. Knecht, W. F. Loomis, A. De Lozanne, and A. Spudich. 1988. Cell motility in *Dictyostelium* amebae lacking myosin heavy chain. *Dev. Biol.* 128:164–177.

Westphal, M., A. Jungbluth, M. Heidecker, B. Mühlbauer, C. Heizer, J.-M. Schwartz, G. Marriot, and G. Gerisch. 1997. Microfilament dynamics during cell movement and chemotaxis monitored using a GFP-actin fusion protein. *Curr. Biol.* 7:176–183.

Yumura, S., H. Mori, and Y. Fukui. 1984. Localization of actin and myosin for the study of amoeboid movement in *Dictyostelium* using improved immunofluorescence. *J. Cell Biol.* 99:894–899.